Magnetohydrodynamic micropolar fluid flow in a porous medium with multiple slip conditions

Ephesus Olusoji Fatunmbi[a,*], Hammed Abiodun Ogunseye[b], Precious Sibanda[b]

[a] Department of Mathematics and Statistics, Federal Polytechnic, Ilaro, Nigeria
[b] School of Mathematics, Statistics and Computer Science, University of KwaZulu-Natal, Private Bag X01, Scottsville, Pietermaritzburg 3209, South Africa

ARTICLE INFO

ABSTRACT

Theoretically, micropolar fluids are used in the biomedical investigations. This study analyzes the flow, heat and mass transfer in a magneto-micropolar reactive fluid over a nonlinear stretching sheet in a saturated non-Darcy porous medium. The impact of velocity, thermal and concentration slips with prescribed surface temperature and concentration boundary conditions are examined. Mathematical models are formulated and solved using an iterative technique spectral quasi-linearization method. The results of numerical simulations are depicted graphically. The present results when cross-checked with earlier reported data in the literature for limiting conditions exhibit good agreement. The results show that the momentum and thermal boundary layer thicknesses fall as the nonlinear stretching parameter increases while the opposite occur with a rise in the thermal conductivity parameter.

1. Introduction

The concept of micropolar and thermo-micropolar fluids as a class of non-Newtonian fluids emanated from the work of Eringen [1,2] and has gained active attention of researchers and scientists because of its significance in several fields of engineering, science and technology. For instance, in bio-medical engineering such as fluid flow in brains and blood flows; metallurgical drawing of filaments, chemical engineering including paint rheology; pharmacodynamics and drug delivery and so on [3,4]. The concept of a micropolar fluid is associated with a group of fluids that manifest certain microscopic properties stemming from the intrinsic structure and micro-movement of the fluid element. They posses microstructural particles which are complex in nature which may be of varying sizes and sometimes contract and/or expand and periodically changing shapes and spin individually. The microstructural pattern of the fluid particles in micropolar fluids, provide a good mathematical framework for simulating the flow attributes of real and complex fluids including polymeric additives, colloidal suspensions, liquid crystals, animal blood, exotic lubricants and so on for which the structure of Navier-Stokes equations of classical hydrodynamic cannot perfectly described [5].

Fluid flow passing a stretching sheet has a lot of interesting industrial and engineering relevant uses such as in the extrusion of plastic sheets, paper and textile production, hot rolling, wire drawing, etc. [6].

The study of such flows evolved from the work of Crane [7] and has been investigated by various researchers analysing the impact of vital parameters on different fluids, geometries, boundary conditions and methods. For instance, Muhammad et al. [8] recently reported on the flow of a viscous ferrofluid passing a linearly stretched sheet influenced by a magnetic dipole. Mahmoud [9] used a micropolar fluid whereas Akbar et al. [10] applied an Eyring-Powell fluid. However, in practical situations, the stretching of sheets is nonlinear , hence, the investigation of fluid flow over a nonlinearly stretched surface by various researchers. Cortell [11–12] presented a numerical study of flow and heat transfer activated by nonlinearly stretched sheet with viscous dissipation and thermal radiation under the influence of both a constant and a prescribed surface temperature as well as a heat flux at the boundary. It was reported that the fluid velocity reduced and the temperature improved as the nonlinear stretching parameter increased. Hayat et al. [13] studied mixed convection flow prompted by a nonlinearly stretched sheet in a micropolar fluid while Waqas et al. [14] improved on the work of [13] by investigating dissipative and Joule heating effects and a convective condition at the boundary.

Furthermore, fluid flow in a porous medium with magnetic field effects and a chemical reaction is important in various engineering operations such as in geothermal energy extractions, MHD generators, thermal insulation engineering, irrigation systems, crude oil extraction, etc. [6,15]. To this end, Pal and Chatterjee [16] numerically examined a

---

flow problem of MHD micropolar fluid with a uniform magnetic field. The authors transformed the governing equations from partial to ordinary differential equations via a similarity conversion analysis and reported that the magnetic and Darcy parameters caused a reduction in the velocity of the fluid. Nadeem et al. [17] reported on the influence of thermal stratification in a porous medium filled with ferromagnetic Jeffrey kind of fluid along a sheet which stretches linearly in the flow direction. Recently, Tripatty et al. [18] investigated a problem based on flow in porous medium of non-Darcian type with the effect of chemical reaction and non-uniform heat source passing a linearly stretching sheet. Their equations were solved numerically by means of a shooting technique combined with the Runge-Kutta method It was underlined in the work that an increase in the porosity and inertial parameters reduced the momentum boundary layer thickness. However, the analysis was performed on assumption of a no-slip condition at the wall which is the core idea of the Navier-Stokes model. For some practical situations however, this assumption fails to hold.

Wang [19] showed that slip flow problems are crucial for stationary and moving walls on particulate fluids such as emulsions and polymer solutions where slip may exist between the fluid and the boundary. The velocity and temperature slip at the boundary surface can be described as discontinuity in the rate of transport phenomenon over the interface which has been proposed over two hundred years ago in lieu of the common no-slip kind of boundary conditions. Fluid slip has significant practical applications, for instance, it helps in reducing flow resistance in micro-channels. Also, in heat transfer processes such as in cooling of electronic devices, fuel cells and heat exchangers, temperature slip also refereed to as thermal jump is crucial in applications. In some thermal systems, a small temperature boundary resistance may be required for enhancing dissipation of heat in electronics while a high thermal slip can be employed for temperature control [20]. On this ground, Kumar et al. [21] examined the flow of dissipative and reactive Casson fluid on a stretching sheet with the influence of multiple slip, radiation and chemical reaction while an analysis of the effects of multiple slip in an unsteady flow passing a vertically stretching plate with radiation and suction/injection influence was reported by Mabood and Shateyi [22]. Similar studies have been made by various scholars owing to the many applications of such flows [23–26]. However, in these studies the slip effects were investigated for a linearly stretching sheet without taking into consideration the case when the stretching of the sheet is nonlinear which is the basis for this research.

This study therefore investigates the impact of velocity, thermal and concentration slips on a nonlinearly stretching sheet in a magneto-micropolar reactive fluid embedded in a porous medium of Darcy-Forchheimer type with surface mass flux. By means of relevant similarity conversion , the flow equations are transformed from partial to ordinary differential equations and then integrated numerically via an iterative technique spectral quasi-linearization method. This problem is an extension to the work of [18] with the following new features:

- It generalizes that of [18] by considering a nonlinearly stretching surface instead of linear surface .
- The assumption of a non-uniform magnetic field as against a uniform magnetic field in [18].
- The inclusion of surface mass flux (suction/injection) in the present work which was not considered in the earlier study [18].
- The investigation of multiple slip conditions at the boundary as against the no-slip conditions examined in [18].
- The cases of Prescribed Surface Temperature (PST) and Prescribed Surface Concentration (PSC) as against a uniform temperature and concentration.

2. The problem formulation and modelled equations

The problem in this study is a steady flow on a two-dimensional nonlinearly stretching permeable sheet in a saturated non-Darcian
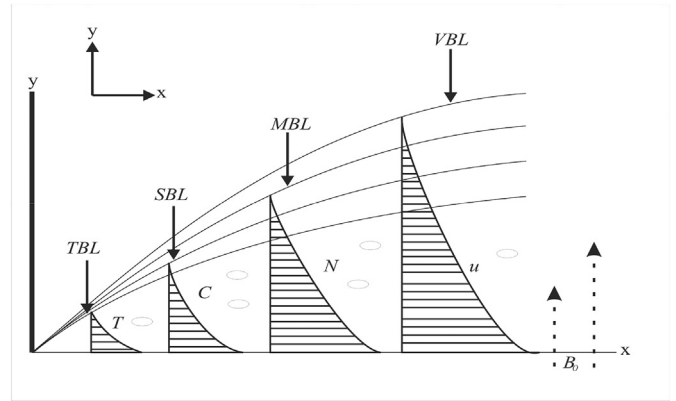

Fig. 1. Flow geometry.

porous medium with the working fluid being an electrically conducting micropolar fluid as described in Fig. 1. A non-uniform magnetic field acts normal to the flow direction with strength $B(x) = B_0 x^{(r-1)/2}$, where x describes the stretching coordinate with velocity component u. The induced magnetic and the electric are not considered and the fluid characteristics are assumed to be isotropic and constant. The velocity component v is normal to the y direction. The stretching sheet velocity varies in a nonlinear manner with slip condition given as $u = u_w + u_s$ where $u_w = cx^r$ with $c > 0$ a constant, r is the power law index, u_s is the slip velocity, the surface temperature is $T_w = T_\infty + Ax^{m_1}$ while the surface concentration is $C_w = C_\infty + Bx^{m_2}$ with m_1 and m_2 representing the surface temperature and concentration parameters respectively. In the flow geometry Fig. 1, TBL, SBL, MBL and VBL respectively refers to thermal, microrotation, solutal and velocity boundary layers.

Incorporating above assumptions with that of boundary layer approximations, the modelled equations are:

$$\frac{\partial u}{\partial x} + \frac{\partial v}{\partial y} = 0 \tag{1}$$

$$u\frac{\partial u}{\partial x} + v\frac{\partial u}{\partial y} = \frac{(\mu + \mu_r)}{\rho}\frac{\partial^2 u}{\partial y^2} + \frac{\mu_r}{\rho}\frac{\partial N}{\partial y} - \frac{\sigma B^2(x)}{\rho}u - \frac{\nu}{K_p}u - \frac{F}{K_p}u^2 \tag{2}$$

$$u\frac{\partial N}{\partial x} + v\frac{\partial N}{\partial y} = \frac{\gamma}{\rho j}\frac{\partial^2 N}{\partial y^2} - \frac{\mu_r}{\rho j}\left(2N + \frac{\partial u}{\partial y}\right) \tag{3}$$

$$u\frac{\partial T}{\partial x} + v\frac{\partial T}{\partial y} = \frac{\kappa_\star}{\rho C_p}\frac{\partial^2 T}{\partial y^2} + \frac{(\mu + \mu_r)}{\rho C_p}\left(\frac{\partial u}{\partial y}\right)^2 + \frac{\sigma B^2(x)}{\rho C_p}u^2 + \frac{q'''}{\rho C_p} \tag{4}$$

$$u\frac{\partial C}{\partial x} + v\frac{\partial C}{\partial y} = Dm\frac{\partial^2 C}{\partial y^2} - k_c(C - C_\infty) \tag{5}$$

The incorporated boundary conditions are:

$$u = u_w + u_s, \ v = V_w, \ N = -h\frac{\partial u}{\partial y}, \ T = T_w + T_s, \ C = C_w + C_s \ at \ y = 0,$$
$$u\longrightarrow 0, \ N\longrightarrow 0, \ T\longrightarrow T_\infty, C\longrightarrow C_\infty \ as \ y \to \infty \tag{6}$$

The non-uniform heat source/sink q''' in the energy Eq. (5) is described by [27]

$$q''' = \frac{\kappa u_w}{x^r \nu}[H(T_w - T_\infty)f' + H^\star(T - T_\infty)] \tag{7}$$

with H and $H^\star$ being the space and heat dependent source/sink respectively. For heat source $H > 0$ and $H^\star > 0$ whereas for heat sink, $H < 0$ and $H^\star < 0$.

In the Eqs. (1)–(5) the spin gradient, dynamic, vortex and kinematic viscosity are indicated by γ, μ, μ_r and ν in that order, while ρ denotes the density and j stands for micro inertial density. Also T indicates the fluid temperature while C is the fluid concentration, N shows the component of microrotation, $\kappa_\star$ is the thermal conductivity whereas K_p denotes the

permeability of the porous medium. Similarly, k_c, σ, C_p, Dm symbolize rate of chemical reaction, electrical conductivity, specific heat at constant pressure and molecular diffusivity in that order. Meanwhile, we take $F = F_0 x^{-1}$, $K_p = K_p{}^\star x^{1-r}$, $H = ax^{r-1}$, $H^\star = bx^{r-1}$, $k_c = k_0 x^{r-1}$ to represent the Forchheimer constant, permeability of the porous medium [28–30].

In Eq. (6), the suction/injection term indicated is $V_w = V_0 x^{(r-1)/2}$ where V_0 is a constant, the slip velocity is indicated by $u_s = c_1 \frac{\partial u}{\partial y}$, the temperature slip is represented by $T_s = c_2 \frac{\partial T}{\partial y}$, the concentration slip is denoted by $C_s = c_3 \frac{\partial C}{\partial y}$ while h connotes surface boundary parameter such that $0 \leq h \leq 1$. A strong concentration is witnessed when $h = 0$ leading to $N = 0$. This describes a situation in which the particle density is large such that in the neighbourhood of the boundary, the micro-particles cannot rotate or translate [31]. On the other hand, the case when $h = 1/2$ is an indication of a weak concentration of micro-particles and the disappearance of nonsymmetric term of the stress tensor [32] whereas $h = 1$ models the flow that is turbulent in nature [33].

The flow equations are transformed from PDEs to ODEs by means of Eq. (8) which also reduce the independent variables x, y to a single variable η [16,34]

$$
\eta = y\left[\frac{c(r+1)x^r}{2x\nu}\right]^{1/2}, \psi = x^{(r-1)/2}\left[\frac{2c\nu}{(r+1)}\right]^{1/2} f(\eta), N
$$

$$
= x^{(3r-1)/2}\left[\frac{c^3(r+1)}{2\nu}\right]^{1/2} g(\eta)
$$

$$
u = cx^r f', v = -\left[\frac{c\nu(r+1)}{2}\right]^{1/2} x^{(r-1)/2}\left(f + \frac{(r-1)}{(r+1)}\eta f'\right)
$$

$$
\theta(\eta) = \frac{T - T_\infty}{T_w - T_\infty}, \Phi(\eta) = \frac{C - C_\infty}{C_w - C_\infty}, \gamma = \left(\mu + \frac{\mu_r}{2}\right)j, j = \left(\frac{\nu}{c}\right)x^{(1-r)}
$$

(8)

With the application of the stream function given as

$$
u = \frac{\partial \psi}{\partial y}, \quad v = -\frac{\partial \psi}{\partial x}
$$

(9)

Eq. (1) is satisfied by Eq. (9). Then substituting Eq. (8) into Eqs. (2)–(6) yields the following:

$$
(1 + K)f''' + ff'' + Kg' - 2\left(\frac{r + F_s}{r + 1}\right)f'^2 - \left(\frac{2}{r + 1}\right)(M + Da)f' = 0
$$

(10)

$$
(1 + K/2)g'' + fg' - \left(\frac{3r - 1}{r + 1}\right)f'g - K(2g + f'')\left(\frac{2}{r + 1}\right) = 0
$$

(11)

$$
\theta'' + Prf\theta' - \left(\frac{2m_1}{r + 1}\right)Prf'\theta + (1 + K)PrEcx^{2r-m_1}f''^2 +
$$

$$
\left(\frac{2}{r + 1}\right)MPrEcx^{2r-m_1}f'^2 + \left(\frac{2}{r + 1}\right)Pr(\alpha f' + \beta\theta) = 0
$$

(12)

However, in order to have purely similarity solution in Eq. (12), we set $m_1 = 2r$ [14,34].
Hence the energy Eq. (12) becomes

$$
\theta'' + Pr\left[f\theta' - \left(\frac{4r}{r + 1}\right)f'\theta\right] + (1 + K)PrEcf''^2 + \left(\frac{2}{r + 1}\right)MPrEcf'^2
$$

$$
+ \left(\frac{2}{r + 1}\right)Pr(\alpha f' + \beta\theta) = 0
$$

(13)

$$
\Phi'' + Scf\Phi' - \left(\frac{2m_2}{r + 1}\right)Sc f'\Phi - \left(\frac{2}{r + 1}\right)Sc\gamma_1\Phi = 0
$$

(14)

Subject to boundary conditions:

$$
\eta = 0: f' = 1 + G_1 f'', f = fw, g = -hf'', \theta = 1 + G_2\theta', \Phi = 1 + G_3\Phi'
$$

(15)

$$
\eta \longrightarrow \infty : f' \longrightarrow 0, \ g \longrightarrow 0, \ \theta \longrightarrow 0, \ \Phi \longrightarrow 0.
$$

(16)

Here $K = \frac{\mu_r}{\mu}$ is the micropolar material parameter, $fw = -\frac{\sqrt{2}V_0}{(\sqrt{c\nu(r+1)})}$ is the suction/injection parameter with $fw > 0$ and $fw < 0$ indicating suction and injection respectively while $fw = 0$, indicates an impermeable sheet. The Darcy and the magnetic field parameters are respectively described by $Da = \frac{\nu}{cK_p{}^\star}$ and $M = \frac{\sigma B_0^2}{c\rho}$. The Prandtl number is $Pr = \frac{\mu C_p}{k_\star}$ and the $Sc = \frac{\nu}{Dm}$ stands for the Schmidt number, $\alpha = \frac{ak}{\mu C_p}$ and $\beta = \frac{bk^\star}{\mu C_p}$ are the space and heat generation/absorption parameters in that order, Fs and $Ec = \frac{c^2}{ACp}$ respectively describe the Forchheimer and Eckert numbers and $\gamma_1 = \left(\frac{k_0}{c}\right)$ indicates the chemical reaction parameter whereas the velocity, thermal and concentration slips parameters are denoted by G_1, G_2 and G_3 in that order. The relevant quantities of engineering importance in this work are the skin friction coefficient C_{fx}, the Nusselt number Nu_x (relating to the transfer of heat at the sheet surface) as well as Sherwood number Sh_x (corresponding to mass transfer at the surface). The corresponding mathematical descriptions are given in Eqs. (17)–(19).

$$
C_{fx} = \frac{\tau_w}{\rho u_w^2}
$$

(17)

$$
Nu_x = \frac{xq_w}{\kappa_\star(T_w - T_\infty)}
$$

(18)

$$
Sh_x = \frac{xq_m}{Dm(C_w - C_\infty)}
$$

(19)

with

$$
\tau_w = \left[(\mu + \mu_r)\frac{\partial u}{\partial y} + \mu_r N\right]_{y=0}, q_w = -\left(\kappa_\star \frac{\partial T}{\partial y}\right)_{y=0}, q_m = -\left(Dm\frac{\partial C}{\partial y}\right)_{y=0}
$$

(20)

where τ_w, q_w and q_m denote the surface shear stress, heat and mass flux in that order. Using Eqs. (8) and (20) the dimensionless skin friction coefficient is

$$
C_{fx} = \left(\frac{r + 1}{2}\right)^{1/2}[1 + (1 - h)K]Re_x^{-1/2}f''(0)
$$

(21)

while the Nusselt and Sherwood numbers respectively simplify to

$$
Nu_x = -\left(\frac{r + 1}{2}\right)^{1/2}Re_x^{1/2}\theta'(0), Sh_x = -\left(\frac{r + 1}{2}\right)^{1/2}Re_x^{1/2}\Phi'(0)
$$

(22)

3. Solution methodology

For the solution methodology, the spectral quasi-linearization method (SQLM) is utilized to numerically integrate the coupled nonlinear differential Eqs. (10), (11), (13) and (14). A concise description of the SQLM can be found in Motsa [35].

In respect to SQLM, Eqs. (10), (11), (13) and (14) are linearized to give the following iterative scheme:

$$
a_{1,n}f'''_{n+1} + a_{2,n}f''_{n+1} + a_{3,n}f'_{n+1} + a_{4,n}f_{n+1} + a_{5,n}g'_{n+1} = R_n^f
$$

(23)

$$
a_{6,n}g''_{n+1} + a_{7,n}g'_{n+1} + a_{8,n}g_{n+1} + a_{9,n}f''_{n+1} + a_{10,n}f'_{n+1} + a_{11,n}f_{n+1}
$$

$$
= R_n^g
$$

(24)

$$
a_{12,n}\theta''_{n+1} + a_{13,n}\theta'_{n+1} + a_{14,n}\theta_{n+1} + a_{15,n}f''_{n+1} + a_{16,n}f'_{n+1} + a_{17,n}f_{n+1}
$$

$$
= R_n^\theta,
$$

(25)

$$
a_{18,n}\Phi''_{n+1} + a_{19,n}\Phi'_{n+1} + a_{20,n}\Phi_{n+1} + a_{21,n}f'_{n+1} + a_{22,n}f_{n+1} = R_n^\Phi
$$

(26)

with corresponding boundary conditions:

$$
f'_{n+1}(0) = 1 + G_1 f''_{n+1}(0), \ f_{n+1}(0) = fw, \ g_{n+1}(0) = -hf''_{n+1}(0)
$$

$$\theta_{n+1}(0) = 1 + G_2\theta'_{n+1}(0), \ \Phi_{n+1}(0) = 1 + G_3\Phi'_{n+1}(0) \qquad (27)$$

$$f'_{n+1}(\infty) = 0, \ g_{n+1}(\infty) = 0, \ \theta_{n+1}(\infty) = 0, \ \Phi_{n+1}(\infty) = 0 \qquad (28)$$

where the coefficients $a_{i,n}$ ($i = 1,...,22$), are defined as:

$$a_{1,n} = (1+K), \ a_{2,n} = f_n, \ a_{3,n}$$
$$= -\frac{1}{r+1}(4(r+F_s)f'_n + 2(M+Da)), \ a_{4,n} = f''_n,$$
$$a_{5,n} = K, \ a_{6,n} = 1 + \frac{K}{2}, \ a_{7,n} = f_n, \ a_{8,n} = \frac{-1}{r+1}((3r-1)f'_n - 4K), \ a_{9,n}$$
$$= -\frac{2K}{r+1},$$
$$a_{10,n} = \frac{-(3r-1)g_n}{r+1}, \ a_{11,n} = g'_n, \ a_{12,n} = 1, \ a_{13,n} = Prf_n, \ a_{14,n}$$
$$= Pr\beta - \frac{4rPrf'_n}{r+1},$$
$$a_{15,n} = 2(1+K)PrEcf''_n, \ a_{16,n} = Pr\alpha - \frac{4Pr}{r+1}[r\theta_n - MEcf'_n], \ a_{17,n}$$
$$= Pr\theta'_n, \ a_{18,n} = 1,$$
$$a_{19,n} = Scf_n, \ a_{20,n} = \frac{-2Sc}{r+1}[m_2f'_n - \gamma_1], \ a_{21,n} = \frac{-2m_2Sc\Phi_n}{r+1}, \ a_{22,n}$$
$$= Sc\Phi'_n$$

$$R_n^f = a_{1,n}f'''_n + a_{2,n}f''_n + a_{3,n}f'_n + a_{4,n}f_n + a_{5,n}g'_n - \Phi_f,$$
$$R_n^g = a_{6,n}g''_n + a_{7,n}g'_n + a_{8,n}g_n + a_{9,n}f'_n + a_{10,n}f'_n + a_{11,n}f_n - \Phi_g,$$
$$R_n^\theta = a_{12,n}\theta''_n + a_{13,n}\theta'_n + a_{14,n}\theta_n + a_{15,n}f''_n + a_{16,n}f'_n + a_{17,n}f_n - \Phi_\theta,$$
$$R_n^\Phi = a_{18,n}\Phi''_n + a_{19,n}\Phi'_n + a_{20,n}\Phi_n + a_{21,n}f'_n + a_{22,n}f_n - \Phi_\Phi,$$
$$R_n^f$$
$$= (1+K)f_{n'''} + ff'' + Kg'_n - 2\left(\frac{r+F_s}{r+1}\right)f'^2_n - \left(\frac{2}{r+1}\right)(M+Da)f'_n$$
$$R_n^g = (1+K/2)g''_n + f_ng'_n - \left(\frac{3r-1}{r+1}\right)f'_ng_n - K(2g_n + f''_n)\left(\frac{2}{r+1}\right),$$
$$R_n^\theta = \theta''_n + Pr\left[f_n\theta'_n - \left(\frac{4r}{r+1}\right)f'_n\theta_n\right] + (1+K)PrEcf$$
$$''^2_n + \left(\frac{2}{r+1}\right)MPrEcf^2_{n'}$$

$$+ \left(\frac{2}{r+1}\right)Pr(\alpha f'_n + \beta\theta_n), \ R_n^\Phi$$
$$= \Phi''_n + Scf_n\Phi'_n - \left(\frac{2m_2}{r+1}\right)Sc\Phi_nf'_n - \left(\frac{2}{r+1}\right)Sc\gamma_1\Phi_n$$

$$(29)$$

Eqs. (23)–(28) make up the SQLM iterative scheme and the equations are numerically solved via the Chebyshev pseudo-spectral technique.

Using the Chebyshev pseudo-spectral collocation method, we discretize Eqs. (23)–(26). Firstly, the semi-infinite domain, $\eta \in [0, \infty)$ is truncated by replacing it with $\eta \in [0, \varpi_\infty]$, where $\varpi_\infty \in \mathbb{Z}^+$.

Secondly, we transform the interval $[0, \varpi_\infty] \longmapsto [-1, 1]$, using the transformation $\eta = \frac{1}{2}(\xi + 1)\varpi_\infty$. The derivatives of the unknown variables $f(\eta)$, $g(\eta)$, $\theta(\eta)$ and $\Phi(\eta)$ are computed using the Chebyshev differentiation matrix D (see Trefethen [36]), at the collocation points as a matrix vector product;

$$\frac{df}{d\eta} = \sum_{i=0}^{\overline{N}} D_{ij}f(\xi_i) = DF, \ j = 0, 1, 2, ..., \overline{N} \qquad (30)$$

where $\overline{N}$ is the number of collocation points, $\mathbf{D} = 2D/\varpi_\infty$ and $F = [f(\xi_0), f(\xi_1),..., f(\xi_{\overline{N}})]^T$ is a vector function at the collocation point. The Gauss-Lobatto points are selected to define the nodes in $[-1, 1]$ as:

$$\xi_k = \cos\left(\frac{\pi k}{\overline{N}}\right), \ k = 0, 1, ..., \overline{N}; \ -1 \le \xi \le 1 \qquad (31)$$

Let Ω, Θ and Φ be a similar vector function representing g, θ and Φ respectively. Then, Higher order derivatives of f, g, θ and Φ are evaluated as powers of $\mathbf{D}$, that is

$$f^s(\eta) = \mathbf{D}^sF, \ g^s(\eta) = \mathbf{D}^s\Omega, \ \theta^s(\eta) = \mathbf{D}^s\Theta, \ \Phi^s(\eta) = \mathbf{D}^s\Phi \qquad (32)$$

Substituting Eqs. (30)–(32) into Eqs. (23)–(26), we obtain the following matrix form:

$$\begin{bmatrix} \Delta_{11} & \Delta_{12} & \Delta_{13} & \Delta_{14} \\ \Delta_{21} & \Delta_{22} & \Delta_{23} & \Delta_{24} \\ \Delta_{31} & \Delta_{32} & \Delta_{33} & \Delta_{34} \\ \Delta_{41} & \Delta_{42} & \Delta_{43} & \Delta_{44} \end{bmatrix} \begin{bmatrix} F_{n+1} \\ \Omega_{n+1} \\ \Theta_{n+1} \\ \Phi_{n+1} \end{bmatrix} = \begin{bmatrix} R_n^f \\ R_n^g \\ R_n^\theta \\ R_n^\Phi \end{bmatrix} \qquad (33)$$

where Δ_{ij} ($i,j = 1,...,2$) are $(\overline{N}+1) \times (\overline{N}+1)$ matrices and R_n^f, R_n^g, R_n^θ and R_n^Φ are $(\overline{N}+1) \times 1$ vectors, such that:

$$\left.\begin{aligned} &\Delta_{11} = \text{diag}[a_{1,n}]\mathbf{D}^3 + \text{diag}[a_{2,n}]\mathbf{D}^2 + \text{diag}[a_{3,n}]\mathbf{D} + \text{diag}[a_{4,n}]\mathbf{I} \\ &\Delta_{13} = \Delta_{14} = 0_{\overline{N}+1\times\overline{N}+1}, \ \Delta_{21} = \text{diag}[\alpha_{9,n}]\mathbf{D}^2 + \text{diag}[\alpha_{10,n}]\mathbf{D} + \\ &\quad \text{diag}[\alpha_{11,n}]\mathbf{I} \\ &\Delta_{22} = \text{diag}[\alpha_{6,n}]\mathbf{D}^2, +\text{diag}[\alpha_{7,n}]\mathbf{D} + \text{diag}[\alpha_{8,n}]\mathbf{I}, \ \Delta_{23} = \Delta_{24} \\ &\quad = 0_{\overline{N}+1\times\overline{N}+1}, \\ &\Delta_{31} = \text{diag}[\alpha_{15,n}]\mathbf{D}^2 + \text{diag}[\alpha_{16,n}]\mathbf{D} + \text{diag}[\alpha_{17,n}]\mathbf{I}, \ \Delta_{32} = 0_{\overline{N}+1\times\overline{N}+1}, \\ &\Delta_{41} = \text{diag}[\alpha_{21,n}]\mathbf{D} + \text{diag}[\alpha_{22,n}]\mathbf{I}, \ \Delta_{42} = \Delta_{43} = 0_{\overline{N}+1\times\overline{N}+1} \\ &\Delta_{44} = \text{diag}[\alpha_{18,n}]\mathbf{D}^2 + \text{diag}[\alpha_{19,n}]\mathbf{D} + \text{diag}[\alpha_{20,n}]\mathbf{I} \end{aligned}\right\}$$

$$(34)$$

subject to the boundary conditions

$$\left.\begin{aligned} &F_{n+1}(\xi_{\overline{N}}) = f_w, \ \Sigma_{i=0}^{\overline{N}}[G_1\mathbf{D}_{\overline{N}i} - \mathbf{D}_{\overline{N}i}^2]F_{n+1}(\xi_{\overline{N}}) = 1, \ \Sigma_{i=0}^{\overline{N}}\mathbf{D}_{0i}F_{n+1}(\xi_0) = 0 \\ &\Sigma_{i=0}^{\overline{N}}[\Omega_{n+1}(\xi_{\overline{N}})\mathbf{I} + h\mathbf{D}_{\overline{N}i}^2F_{n+1}(\xi_{\overline{N}})] = 0, \ \Omega_{n+1}(\xi_0) = 0, \\ &\Sigma_{i=0}^{\overline{N}}[\mathbf{I}_{\overline{N}i} - G_2\mathbf{D}_{\overline{N}i}]\Theta_{n+1}(\xi_{\overline{N}}) = 1, \ \Theta_{n+1}(\xi_0) = 0, \\ &\Sigma_{i=0}^{\overline{N}}[\mathbf{I}_{\overline{N}i} - G_3\mathbf{D}_{\overline{N}i}]\Phi_{n+1}(\xi_{\overline{N}}) = 1, \ \Phi_{n+1}(\xi_0) = 0 \end{aligned}\right\}$$

$$(35)$$

The SQLM scheme is initialized with the following approximations;

$$f_0(\eta) = f_w + \left(\frac{1}{1+G_1}\right)(1 - \exp(-\eta)), \ g_0(\eta) = \frac{h}{1+G_2}\exp(-\eta)$$
$$\theta_0(\eta) = \frac{1}{1+G_2}\exp(-\eta), \ \Phi_0(\eta) = \frac{1}{1+G_3}\exp(-\eta)$$

$$(36)$$

4. Validation of results

To check the accuracy and validate the numerical code, the computational values obtained for selected controlling parameters were cross-checked with existing related studies in the literature for limiting cases. Table 1 shows the comparative analysis of the skin friction coefficient C_{fx} obtained using the SQLM with results obtained in [9] via the FEM for different K when $r = 1$, $\lambda = \varphi = M = G_1 = 0$. Similarly, for the variation in the non-linear stretching parameter r we have compared the values of C_{fx} with those reported in [15] obtained using the homotopy analysis method (HAM) when $K = \lambda = \varphi = M = fw = 0$

To further validate the accuracy of our results, the heat transfer rates Nu_x are compared with studies of Grubka and Bobba [37] and Chen [38]. Tables 1 and 2 show that the current results compare favourably with the previous findings in some limiting conditions.

5. Results and discussion

Here, we have plotted the graphs showing the influence of main

Table 1

Comparison of C_{fx} with existing results for changes in r when $K = \lambda = Ec = M = Da = Fs = G_1 = 0$ and $fw = 0$.

K	[9]	Present	r	[15]	Current study
0.0	1.000008	1.00000837	00	0.627555	0.627555
1.0	1.367996	1.36799627	0.2	0.766837	0.766837
2.0	1.621575	1.62157505	0.5	0.889544	0.889544
3.0	1.827392	1.82738216	1.0	1.000000	1.000008
4.0	2.005420	2.00542027	1.5	1.061601	1.061601
			3.0	1.148593	1.148593
			7.0	1.216850	1.216850
			10.0	1.234875	1.234875
			20.0	1.257424	1.257424
			100.0	1.276774	1.276774

Table 2

Comparison of values of Nu_x for changes in Pr when $K = \lambda = Ec = M = G_2 = \alpha = \beta = fw = 0$ and $r = 1$.

Pr	[37]	[38]	Present
0.01	0.0294	0.02942	0.02836573
0.72	1.0885	1.08853	1.08862246
1.0	1.3333	1.33334	1.33333334
3.0	2.5097	2.50972	2.50972158
10.0	4.7969	4.79686	4.79687061
100.0	15.7120	15.7118	15.71196466

controlling parameters on the dimensionless velocity, microrotation, temperature, concentration as well as that of skin friction coefficient C_{fx} and Nusselt number Nu_x. The default values of the parameters used are $K = F_s = Ec = m_2 = 1$, $r = 1.5$, $Pr = 0.7$, $Sc = 0.5$, $M = Da = \alpha = \beta = \gamma_1 = G_1 = f_w = h = G_2 = G_3 = 0.2$, unless otherwise stated.

Figs. 2-3 show the impact of the material (micropolar) parameter K on the velocity and microrotation fields respectively. It is evidently shown that the hydrodynamic and the microrotation boundary layer thickness become thick with a rise in the magnitude of K. This in turn leads to an increase in the velocity field as well as the microrotation profiles. Fig. 2 also indicates that the velocity of the micropolar fluid
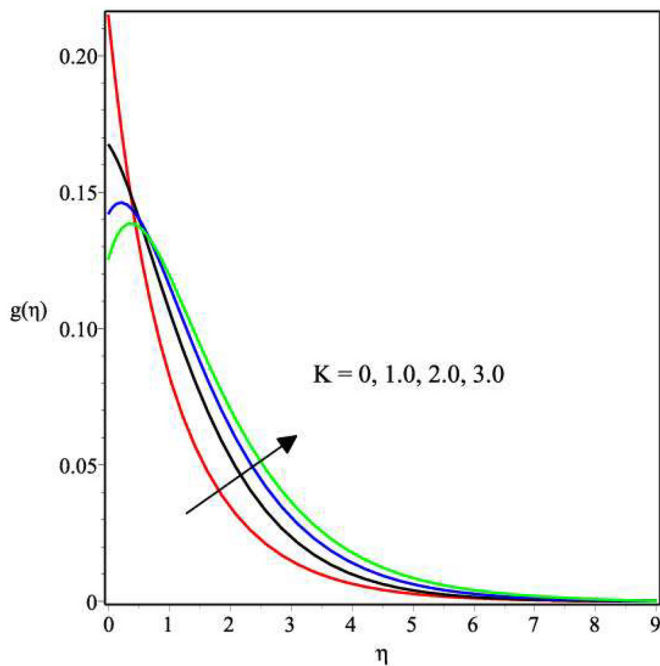

Fig. 3. Influence of K on microrotation profiles.

Fig. 4. Influence of M on velocity profiles.

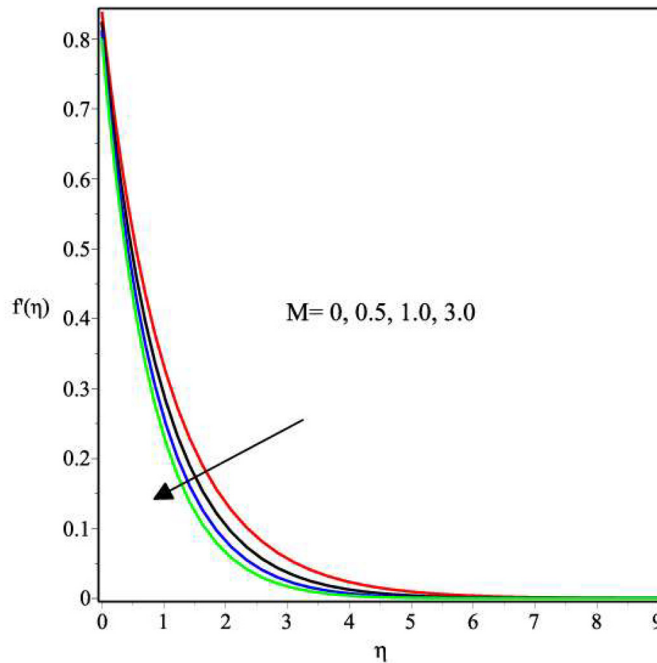**Fig. 2.** Impact of K on velocity profiles.

($K \neq 0$) is higher than that of the classical Newtonian fluid ($K = 0$). Figs. 4 and 5 respectively show the impact of the magnetic field parameter M on the velocity and temperature functions. In Fig. 4, the fluid motion reduces as M increases. This is occasioned by the fact that an application of transverse magnetic field on the fluid which is electrically conducting introduces a resistive Lorentz force which acts against the fluid flow. However, the removal of magnetic field effect ($M = 0$) induces a higher velocity as seen in Fig. 4. On the other hand, in the presence of a magnetic field, some material properties such as the temperature increase owing to the influence of M which reduces the flow velocity and increases the entropy generation. For this reason, the temperature profiles increase with an increase in M as seen in Fig. 5.
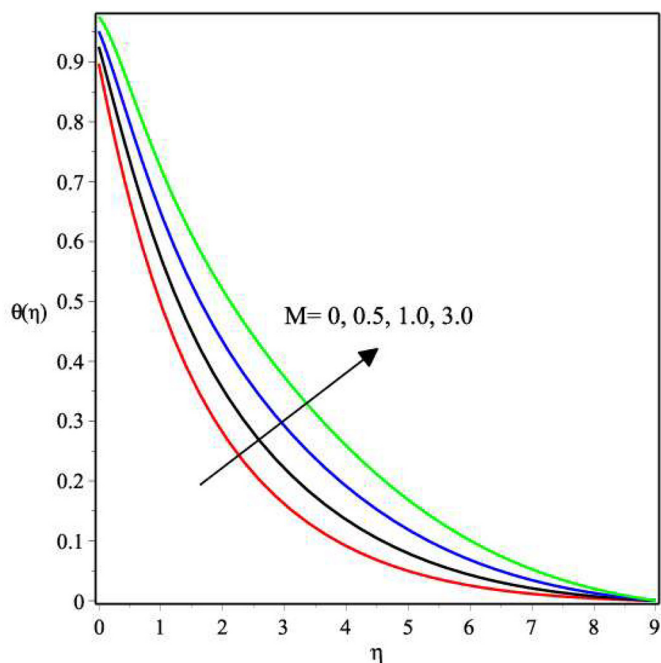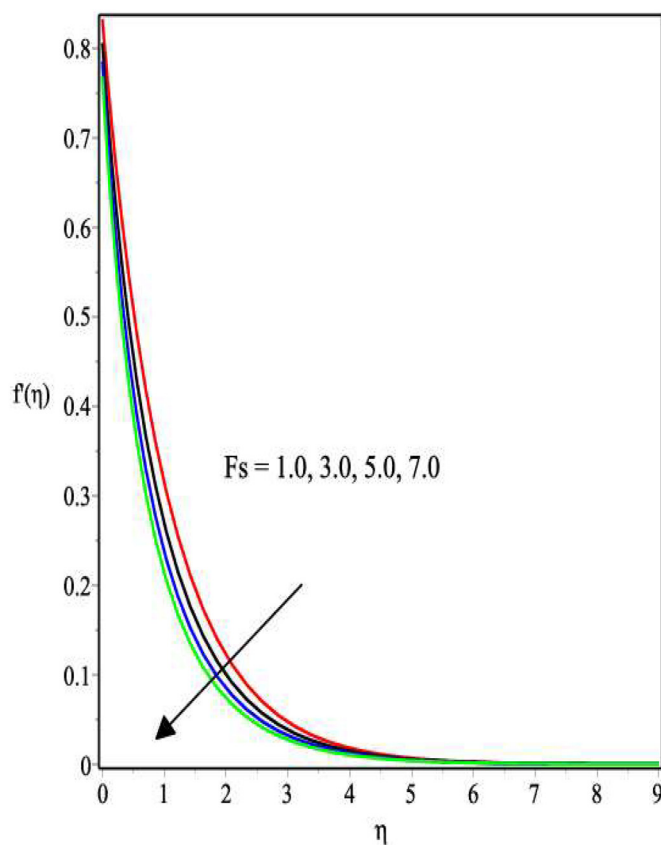
Fig. 5. Impact of *M* on temperature profiles.

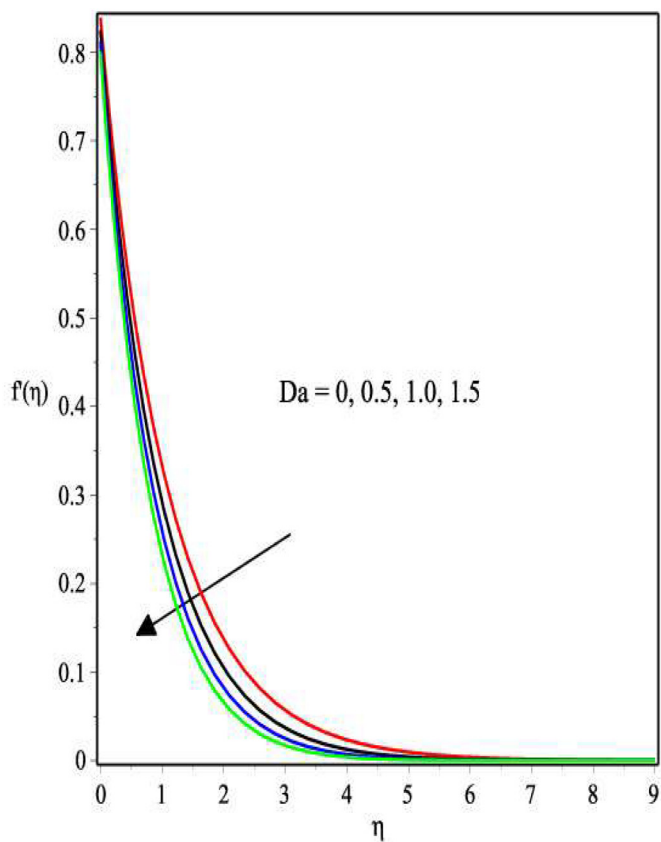**Fig. 6.** Impact of *Da* on velocity profiles.

Fig. 7. Variation of *Fs* with velocity profiles.

In a similar manner, Fig. 7 demonstrates that the influence of the Forchheimer number on the velocity field is the same as that of *Da*. Hence, an increase in these two parameters reduces the fluid flow. The changes in the Eckert number *Ec* corresponding to viscous dissipation with temperature are shown in Fig. 8. Here, the temperature field is enhanced as *Ec* rises. This trend can be explained in that as *Ec* rises, heat
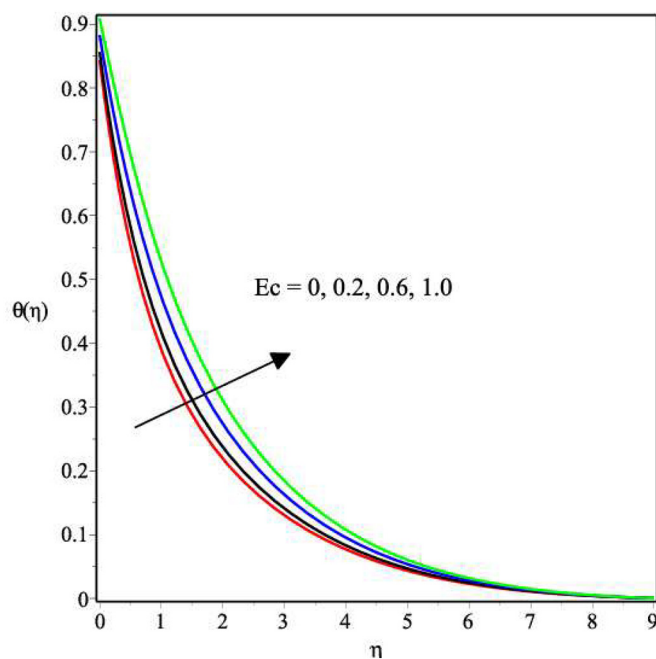
Fig. 8. Response of temperature with *Ec*.

In Fig. 6 the variation of the Darcy number *Da* with the velocity field is shown. it is noted that the impact of *Da* is to dampen the momentum boundary layer thickness and as well as reduce the motion of the fluid due to increase in the resistance to the fluid flow.

More so, the velocity is higher in the absence of the porous medium ($Da = 0$) than when $Da \neq 0$.
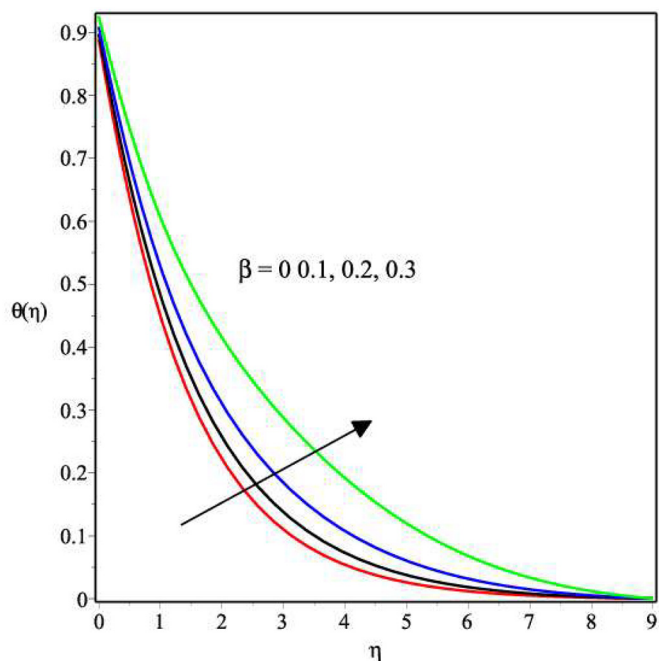
Fig. 9. Influence of β on temperature profiles.
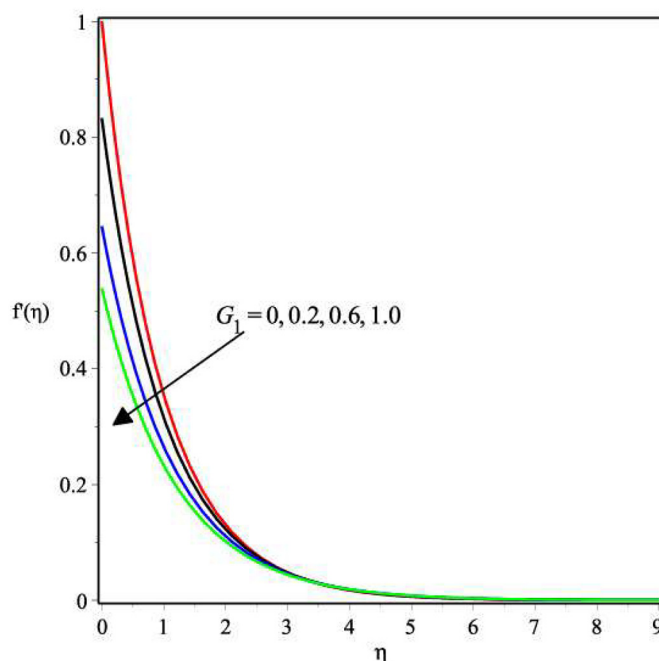
Fig. 11. Reaction of velocity profiles with G_1.

Fig. 10. Impact of γ_1 on concentration.

increase in the slip parameter, with the no-slip situation ($G_1 = 0$) having a higher velocity than when there is velocity slip. This is in line with the earlier results by [25]. The hydrodynamic boundary layer becomes thin as observed as a result of the imposition of the velocity slip condition. The momentum generated by the nonlinear stretching sheet is transferred to the micropolar fluid. However, further from the sheet, the profiles overlap and the effect of the slip is no longer noticeable.

The impact of varying the thermal slip parameter on the temperature characteristics across the boundary layer is shown in Fig. 12. The thermal boundary layer thickness reduces as G_2 continues to increase.
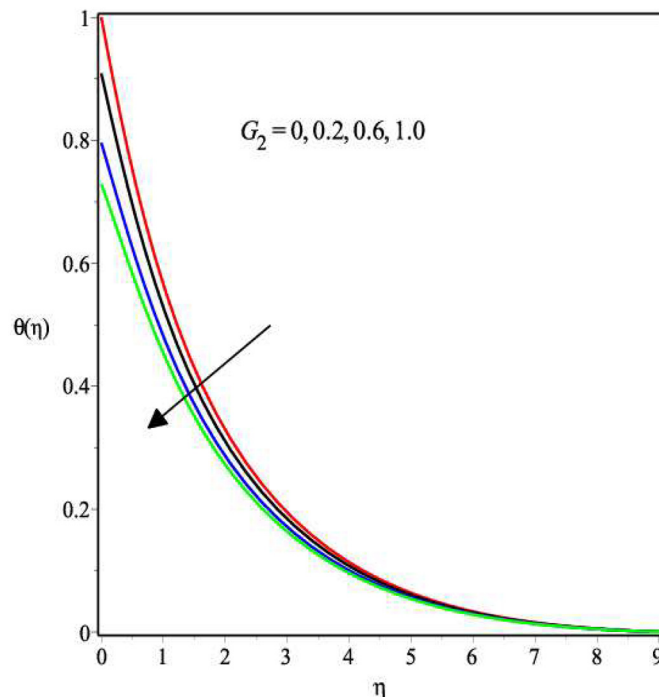

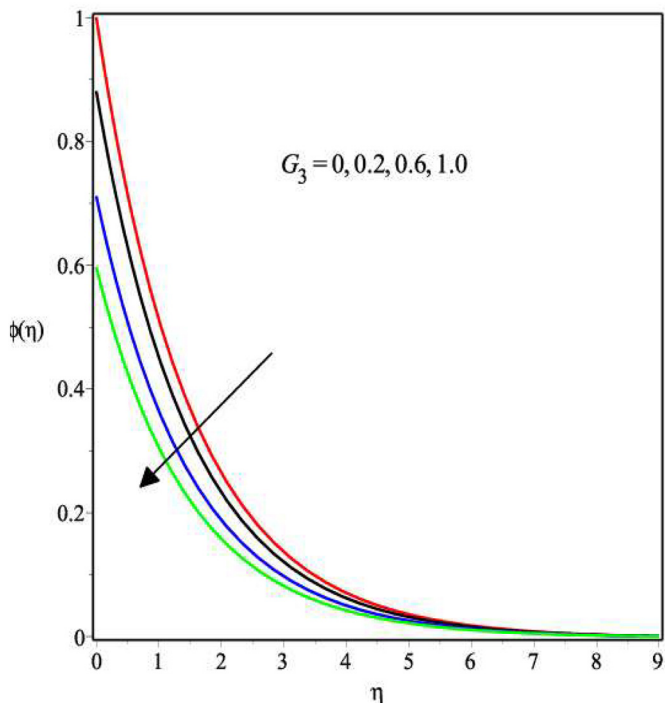**Fig. 12.** Impact of G_2 on temperature.

is produced as a result of the drag between the fluid particles, thus, heat production inside the fluid rises with additional heating due to viscous dissipation. Likewise, Fig. 9 shows the effect of the temperature-dependent heat source β on the temperature distribution. The parameter β produces additional heating which leads to a rise in the fluid temperature. The changes that occur in the concentration field with changes in the chemical reaction parameter γ_1 is given in Fig. 10. In this case, the solutal boundary layer thickness becomes thin as γ_1 increases leading to a reduction in the concentration profiles. In the absence of γ_1, however, higher concentration profiles are observed. The velocity profiles against η for changes in the velocity slip parameter G_1 are shown in Fig. 11. Here, the motion of the fluid is reduced with an

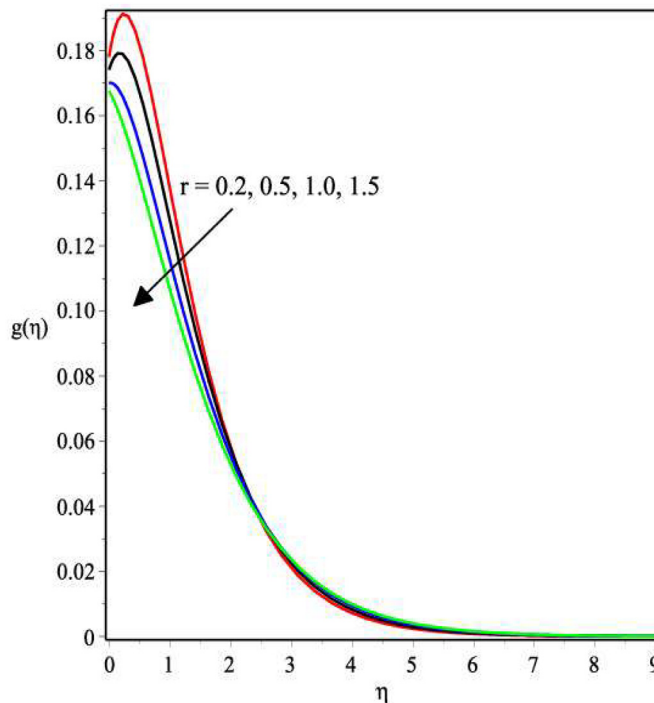**Fig. 13.** Effect of G_3 on concentration profiles.

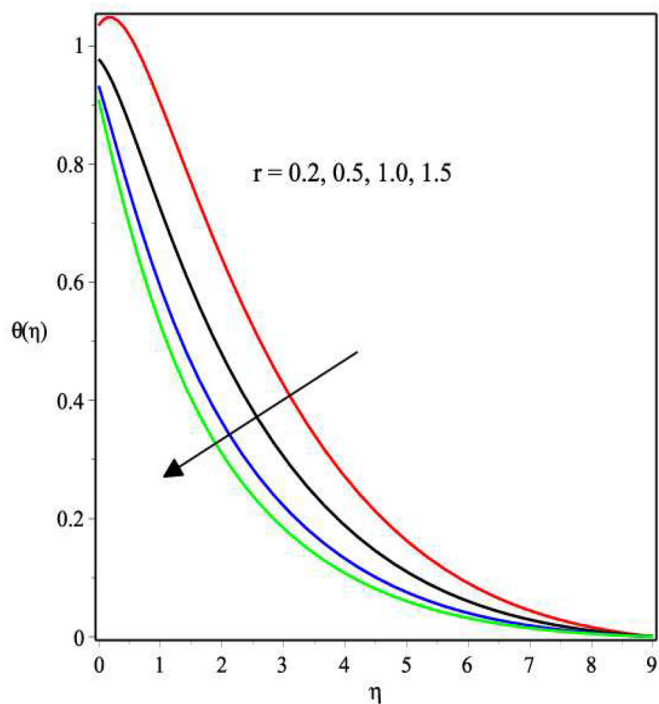**Fig. 15.** Impact of r on microrotation field.

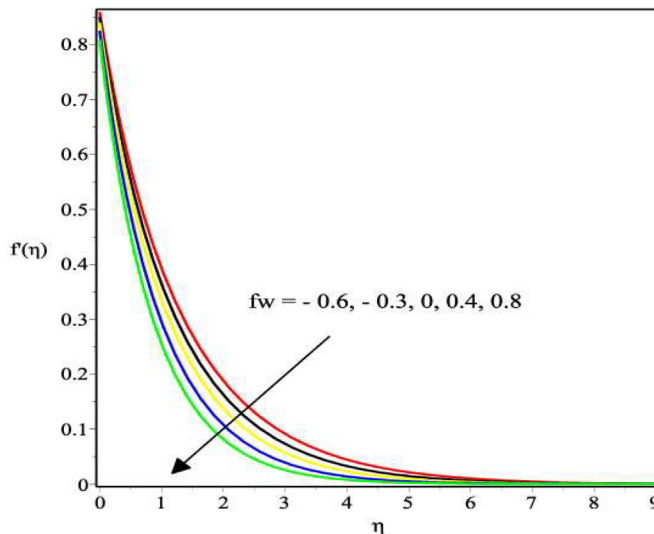**Fig. 14.** Dependence of temperature on r.

Fig. 16. Velocity field for changes in fw.

As a result, the rate at which heat is transferred from the sheet to the fluid drops and hence, a decrease in the temperature distribution occurs. In like manner, Fig. 13 shows that the concentration profiles behave the same way as observed in Fig. 12 when the concentration slip parameter G_3 increases in magnitude. In fact, slip tends to reduce the fluid flow and consequently acts to dampen the net molecular movement and as such the thermal and concentration distributions are reduced. Increasing the nonlinear stretching parameter r reduces the temperature distribution as shown in Fig. 14. In the same way, the

microrotation profiles diminishe with an increase in r as seen in Fig. 15. Figs. 16-17 show the response of both the velocity and temperature fields with changes in the suction/injection parameter fw. In both cases, an increase in suction $fw > 0$ reduces the momentum and thermal boundary layer thicknesses, as seen in Fig. 16 and Fig. 17. However, the opposite behaviour is observed as the injection parameter $fw < 0$ increases.

Figs. 18-19 show the combined impact of the nonlinear stretching r and the material parameter K on C_{fx} and Nu_x. It can be observed from Fig. 18 that increasing values of r leads to a decrease in the skin friction coefficient but for a fixed r, increasing K tends to cause an increase in C_{fx}.

We note also that the rate of heat transfer at the surface Nu_x appreciates with a rise in r as shown in Fig. 19. Similarly, Nu_x increases slightly with a rise in the magnitude of K for a fixed value of r.
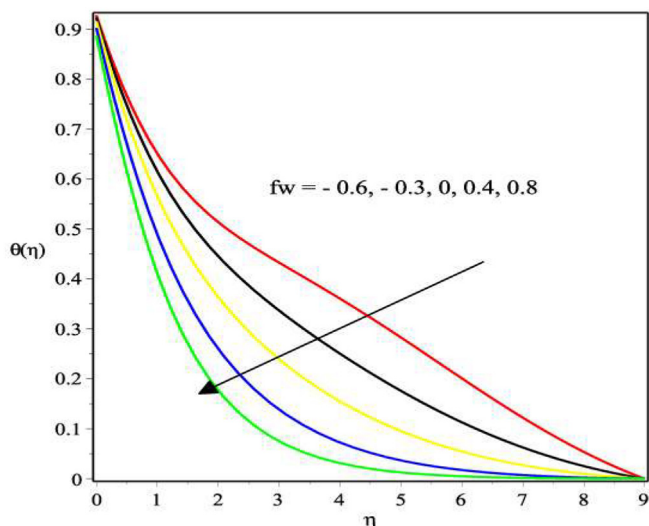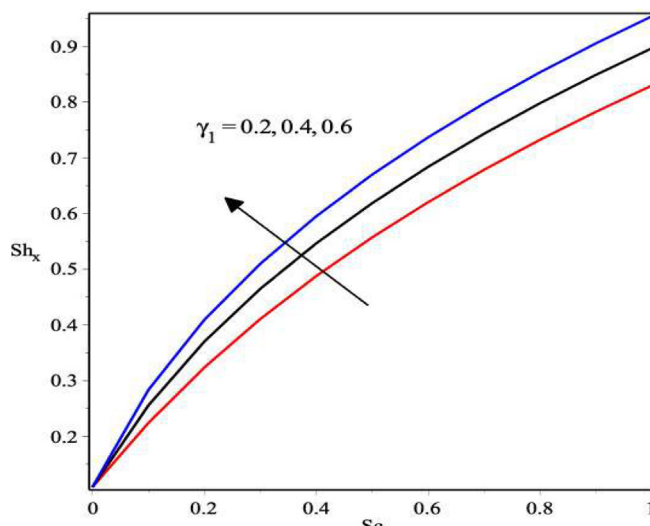
Fig. 17. Variation of *fw* on temperature field.
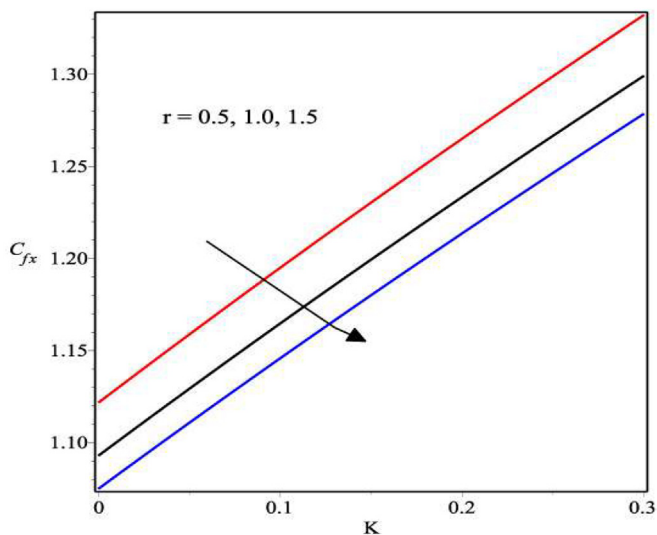

Fig. 20. Variation of γ_1 & *Sc* on Sh_x.
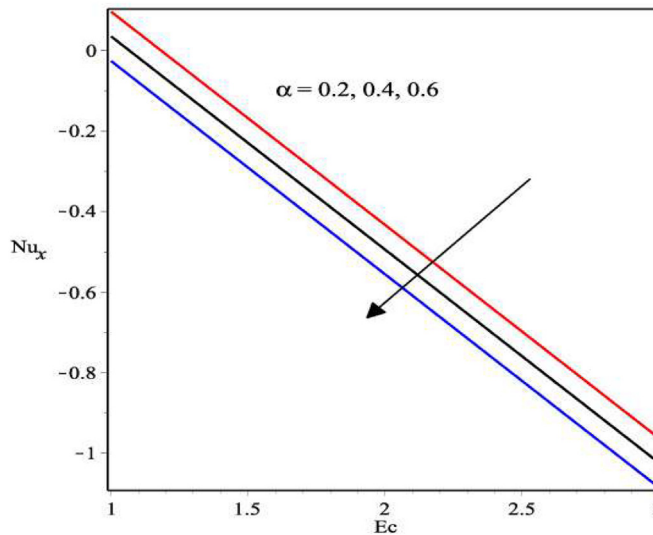

Fig. 18. Variation of *r* & *K* on C_{fx}.

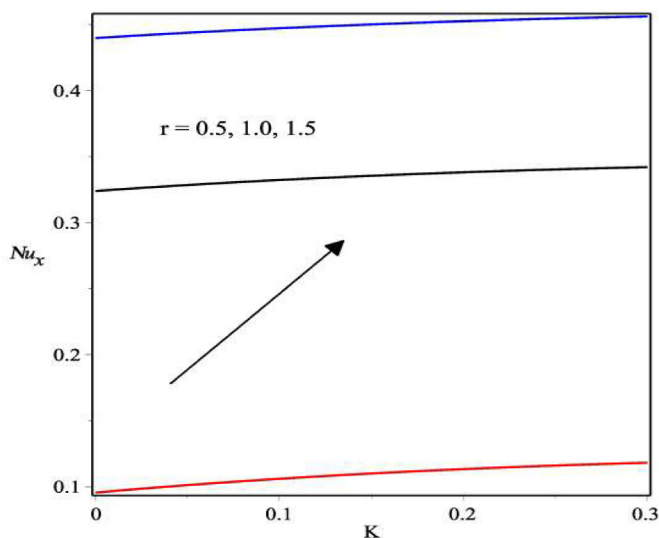**Fig. 21.** Reaction of Nu_x with α & *Ec*.

The change in the Sherwood number Sh_x with the Schmidt number *Sc* and a variation in the chemical reaction parameter γ_1 is displayed in Fig. 20. Observation shows that mass transfer at the surface grows with a rise in both γ_1 and *Sc* parameters. The change in the Nusselt number Nu_x with changes in the space dependent heat source α and the Eckert number *Ec* is given in Fig. 21. Here, both α and *Ec* reduce Nu_x.

6. Conclusion

This study has investigated the flow of a magneto-micropolar reactive fluid past a nonlinear permeable stretching sheet in a porous medium with multiple slips at the boundary. The flow equations were simplified by means of similarity transformations and solved using the iterative spectral quasi-linearization method. Validation of the numerical code was by means of comparison of the results with existing results in the literature for selected parameters. The impact of important physical parameters on the fluid properties and heat transfer was determined and discussed. The following points have been observed:

- The velocity and microrotation profiles increase as the micropolar parameter *K* rises in value. The velocity of micropolar fluid ($K \neq 0$) is comparatively higher than that of a Newtonian fluid ($K = 0$).

Fig. 19. Impact of *r* & *K* on Nu_x.

However, the magnetic field tends to reduce the fluid velocity while enhancing the temperature distribution.

- The thickness of the momentum boundary layer reduces and the flow field decreases with a rise in the velocity slip parameter. The thermal and solutal fields also fall with thermal and solutal slips respectively.

- As the nonlinear stretching parameter r grows in magnitude, the skin friction coefficient C_{fx} diminishes whereas the heat transfer at the sheet surface Nu_x grows as r rises.

- The mass transfer at the sheet surface is enhanced by an increasing first order chemical reaction parameter γ_1 while the heat transfer tends to drop as the space dependent heat source α increases.

Declaration of Competing Interest

None.

References

[1] A.C. Eringen, Theory of micropolar fluids, J. Math. Anal. Appl. 16 (1966) 1–18.
[2] A.C. Eringen, Theory of thermo-microfluids, J. Math. Anal. Appl. 38 (1972) 480–496.
[3] Rana U.S. Reena, Effect of dust particles on rotating micropolar fluid heated from below saturating a porous medium, Appl. Appl. Math. 4 (2009) 189–217.
[4] M.M. Rahman, Convective flows of micropolar fluids from radiate isothermal porous surface with viscous dissipation and joule heating, Commun. Nonlinear Sci. Numer. Simul. 14 (2009) 3018–3030.
[5] G. Lukaszewicz, Micropolar Fluids: Theory and Applications, 1st ed., (1999) (Birkhauser Boston).
[6] S. Ahmad, S. Nadeem, N. Muhammad, Boundary layer flow over a curved surface imbedded in porous medium, Commun. Theor. Phys. 71 (2019) 1–6.
[7] L.J. Crane, Flow past a stretching plate, Commun. Breves 21 (1970) 645–647.
[8] N. Muhammad, S. Nadeem, Sohail Nadeem, M.T. Mustafa, Impact of magnetic dipole on a thermally stratified ferrofluid past a stretchable surface, J. Process Mech. Eng. 0 (0) (2018) (1â€"7).
[9] M.A.A. Mahmoud, Thermal radiation effects on MHD flow of a micropolar fluid over a stretching surface with variable thermal conductivity, Physica A 375 (2007) 401–410.
[10] N.S. Akbar, A. Ebaid, Z.H. Khan, Numerical analysis of magnetic field effects on Eyring-Powell fluid flow towards a stretching sheet, J. Magn. Magn. Mater. 382 (2015) 355–358.
[11] R. Cortell, Viscous flow and heat transfer over a nonlinearly stretching sheet, Appl. Math. Comput. 184 (2007) (864â€"873).
[12] R. Cortell, Effects of viscous dissipation and radiation on the thermal boundary layer over a nonlinearly stretching sheet, Phys. Lett. A 372 (2008) (631â€"636).
[13] T. Hayat, Z. Abbas, T. Javed, Mixed convection flow of a micropolar fluid over a non-linearly stretching sheet, Phys. Lett. A 372 (2008) 637–647.
[14] M. Waqas, M. Farooq, M.J. Khan, A. Alsaedi, T. Hayat, T. Yasmeen, Magnetohydrodynamic (MHD) mixed convection flow of micropolar liquid due to nonlinear stretched sheet with convective condition, Int. J. Heat Mass Transf. 102 (2016) (766 â€" 772).
[15] S. Nadeem, I. Raishad, N. Muhammad, M.T. Mustafa, Mathematical analysis of ferromagnetic fluid embedded in a porous medium, Results Phys. (2017), https://doi.org/10.1016/j.rinp.2017.06.007.
[16] D. Pal, S. Chatterjee, Heat and mass transfer in MHD non-Darcian flow of a micropolar fluid over a stretching sheet embedded in a porous media with non-uniform heat source and thermal radiation, Commun. Nonlinear Sci. Numer. Simul. 15 (2010) 1843–1857.
[17] S. Nadeem, N. Muhammad, Impact of stratification and Cattaneo-Christov heat flux in the flow saturated with porous medium, J. Mol. Liq. (2016), https://doi.org/10.1016/j.molliq.2016.10.006.
[18] R.S. Tripathy, G.C. Dash, S.R. Mishra, M.M. Hoque, Numerical analysis of hydromagnetic micropolar fluid along a stretching sheet embedded in porous medium with non-uniform heat source and chemical reaction, Eng. Sci. Technol. 19 (2016) 1573–1581.
[19] C.Y. Wang, Flow due to stretching boundary with partial Slip-an exact solution of the Navier stokes equation, Chem. Eng. Sci. 57 (2002) 3745–3747.
[20] J.J. Shu, J.M. Teo, W.K. Chan, Fluid velocity slip and temperature jump at a solid surface, Appl. Mech. Rev. 69 (2) (2017) 1–13.
[21] G.V. Kumar, V.M.S.S. Kiran Kumar R, S.V.K. Varma, Multiple slips and chemical reaction effects on mhd stagnation point flow of casson fluid over a stretching sheet with viscous and joules heating, Front. Heat Mass Transf. 10 (23) (2017) 1–9.
[22] F. Mabood, S. Shateyi, Multiple slip effects on MHD unsteady flow heat and mass transfer impinging on permeable stretching sheet with radiation, Model. Simul. Eng. 2019 (2019) 1–11.
[23] H.I. Anderson, Sip flow past a stretching surfcace, Acta Mech. 158 (2002) 121–125.
[24] M. Awais, T. Hayat, A. Ali, S. Irum, Velocity, thermal and concentration slip effects on a magneto-hydrodynamic nanofluid flow, Alexandria Eng. J. 55 (2016) (2107â€"2114).
[25] I. Ullah, S. Shafie, I. Khan, Effects of slip condition and Newtonian heating on MHD flow of Casson fluid over a nonlinearly stretching sheet saturated in a porous medium, J. King Saud Univ. Sci. 29 (2017) (250â€"259).
[26] E.O. Fatunmbi, A. Adeniyan, Heat and mass transfer in MHD micropolar fluid flow over a stretching sheet with velocity and thermal slip conditions, Open J. Fluid Dyn. 8 (2018) 195–215.
[27] D. Pal, H. Mondal, Effect of Soret Dufour, chemical reaction and thermal radiation on MHD non-Darcy unsteady mixed convective heat and mass transfer over a stretching sheet, Commun. Nonlinear Sci. Numer. Simul. 16 (2011) 1942–1958.
[28] O.D. Makinde, Second law analysis for variable viscosity hydromagnetic boundary layer flow with thermal radiation and Newtonian heating, Entropy 13 (2011) 1446–1464.
[29] A. Ishak, Similarity solutions for flow and heat transfer over a permeable surface with convective boundary condition, Appl. Math. Comput. 217 (2010) 837–842.
[30] M.H. Yazdi, S. Abdulaah, I. Hashim, K. Sopian, Effects of viscous dissipation on the slip MHD flow and heat transfer past aa permeable surface with convective boundary condtions, Energies 4 (2011) 2273–2294.
[31] S.K. Jena, M.N.N. Mathur, Similarity solutions for laminar free convection flow of a thermomicropolar fluid past a non-isothermal flat plate, Int. J. Eng. Sci. 19 (1981) 1431–1439.
[32] G. Ahmadi, Self-similar solution of incompressible micropolar boundary layer flow over a semi-infinite plate, Int. J. Eng. Sci. 14 (1976) 639–646.
[33] J. Peddieson, An application of the micropolar model to the calculation of a turbulent shear flow, Int. J. Eng. Sci. 10 (1972) 23–32.
[34] K.L. Hsiao, Heat and mass transfer for micropolar flow with radiation effect past a nonlinearly stretching sheet, Heat Mass Transf. 46 (2010) 413–419.
[35] S.S. Motsa, A new spectral local linearization method for nonlinear boundary layer flow problems, J. Appl. Math. 1 (2013) (Article ID 423628, 15 pages).
[36] L.N. Trefethen, Spectral methods in MATLAB, Siam 10 (2000).
[37] L.J. Grubka, K.M. Bobba, Heat transfer characteristic of a continuous stretching surface with variable temperature, J. Heat Transf. 107 (1985) 248–250.
[38] C.H. Chen, Laminar mixed convection adjacent to vertical continuously stretching sheets, Heat Mass Transf. 33 (1998) 471–476.